



Published in final edited form as:

*Exp Neurol.* 2012 July ; 236(1): 6–18. doi:10.1016/j.expneurol.2012.02.006.

## The Lateral Thoracic Nerve and The Cutaneous Maximus Muscle – A Novel *In Vivo* Model System For Nerve Degeneration And Regeneration Studies

BaoHan Pan<sup>1,3,\*</sup>, Benedikt Grünewald<sup>2</sup>, Thien Nguyen<sup>1</sup>, Mohamed Farah<sup>1</sup>, Michael Polydefkis<sup>1</sup>, John McDonald<sup>1,3</sup>, Lawrence P. Schramm<sup>4,5</sup>, Klaus V. Toyka<sup>1,2</sup>, Ahmet Höke<sup>1,5,\*</sup>, and John W. Griffin<sup>1,5,†</sup>

<sup>1</sup>Department of Neurology, Johns Hopkins University, Baltimore, USA

<sup>2</sup>Department of Neurology, University of Würzburg, Würzburg, Germany

<sup>3</sup>International Center for Spinal Cord Injury, Kennedy Krieger Institute, Baltimore, USA

<sup>4</sup>Department of Biomedical Engineering, Johns Hopkins University, Baltimore, USA

<sup>5</sup>Department of Neuroscience, Johns Hopkins University, Baltimore, USA

### Abstract

We report a novel *in vivo* mouse model system to study regeneration of injured motor nerve and spatiotemporal pattern of denervation in experimental nerve diseases. The lateral thoracic nerve (LTN), as a pure motor nerve, innervates the cutaneous maximus muscle (CMM) by some of the shortest and the longest motor nerve fibers in the mouse body. Its branches and nerve terminals can be imaged in whole mount preparations. Here we describe the branching pattern of the LTN and its innervation of the CMM, and characterize degeneration and regeneration over time after a LTN crush by morphological and electrophysiological analyses. We demonstrate the utility of this model in a well-established neurotoxicity paradigm and in a genetic disease model of the peripheral neuropathy. Furthermore, this system enables punch biopsies that allow repeated and multi-location examinations for LTN regeneration and CMM reinnervation over time. The presence of the LTN and the CMM in a variety of species and its easy accessibility suggests that this *in vivo* model system offers considerable promise for future nerve degeneration and regeneration research.

---

© 2012 Elsevier Inc. All rights reserved.

\*Corresponding authors: Ahmet Höke, Department of Neurology, Johns Hopkins University, The John G. Rangos Sr. Building, 855 N. Wolfe St., Neurology 248, Baltimore, MD, 21205, USA, Phone: 1-410-955-2227 (Office), Phone: 1-410-955-3794 (Laboratory), Fax: 1-410-502-5459, ahoke@jhmi.edu. Baohan Pan, International Center for Spinal Cord Injury, Kennedy Krieger Institute, 707 N Broadway, Rm 516A, Baltimore, MD 21205, USA, Phone: 1-443-923-9191, Fax: 1-443-923-9245, bpan2@jhmi.edu.

†Deceased

#### AUTHOR CONTRIBUTIONS

J.W.G., B.P., A.H. and K.V.T. designed the study. B.P., B.G., M.F. and K.V.T. performed the experiments. B.P., K.V.T. and A.H. wrote the paper with help from L.P.S., T.N., M.P. and J.M.

#### COMPETING FINANCIAL INTERESTS

The authors declare no competing financial interests.

**Publisher's Disclaimer:** This is a PDF file of an unedited manuscript that has been accepted for publication. As a service to our customers we are providing this early version of the manuscript. The manuscript will undergo copyediting, typesetting, and review of the resulting proof before it is published in its final citable form. Please note that during the production process errors may be discovered which could affect the content, and all legal disclaimers that apply to the journal pertain.

## Keywords

lateral thoracic nerve; cutaneous maximus muscle; cutaneous sensory nerve; nerve regeneration; nerve degeneration; neuromuscular junction

---

## INTRODUCTION

Peripheral nerves have the capacity to regenerate after injury but functional recovery remains often incomplete in afflicted patients. The spatiotemporal sequence of simple Wallerian degeneration after nerve injury or in some natural disorders remains a source of controversy (Beirowski et al., 2005; George et al., 1994; Lubiska, 1977; Lunn et al., 1990). Intensive research has focused on the molecules that promote or inhibit regeneration, including transcription factors and specific growth-related proteins produced in the nerve cell bodies following injury, growth factors and other products produced by denervated Schwann cells, proinflammatory and growth factors secreted by infiltrating inflammatory cells, including complement components and antibodies that may inhibit regeneration, and the extracellular matrix of the endoneurium (Fu and Gordon, 1997; Griffin et al., 1996; Hall, 2001; Heine et al., 2004; Höke, 2006; Raivich and Makwana, 2007). Widely used genetically engineered mice now offer a tool for detailed studies into the relative role of most of these factors and this warrants practical and reliable techniques applicable to pure motor nerves. In the most widely used system, sciatic nerve injury, simple axonal pathology gives no information about differential regeneration of specific fiber types because of its mixed composition of fibers, nor can the possible effects of sensory axons and of their adjacent milieu on the regeneration of adjacent motor nerve fibers be easily assessed.

Here we introduce a new model system to study motor nerve degeneration and regeneration that is more easily carried out in the mouse than most previous models of nerve degeneration and regeneration. Many mammals, including the most commonly used laboratory rodents, exhibit a localized reflex twitch of the skin over the back in response to focal cutaneous stimulation. This reflex is generated by contraction of a thin, subdermal muscle that covers most of the back and flank of the trunk. This muscle has been named amongst others cutaneous trunci muscle or cutaneous maximus muscle (CMM). The CMM is innervated by the lateral thoracic nerve (LTN), which is derived from the brachial plexus. Its motor neurons are located in the spinal cord at the level of cervical root 7 (C7) to thoracic root 1 (T1) (Krogh and Towns, 1984; Theriault and Diamond, 1988a, 1988b). The afferents of the CMM reflex arc consist of the anatomically separated dorsal and lateral cutaneous nerves that arise from the dorsal root ganglia (DRG) at each segment of the trunk (Krogh and Towns, 1984; Theriault and Diamond, 1988a). The afferent input synapses in the spinal cord dorsal horn, and the second order fibers ascend to the cervical cord and brainstem (Holstege and Blok, 1989), as well as direct synapses on motor neurons innervating the CMM located in the C7-T1 spinal cord level (Giovannelli Barilari and Kuypers, 1969). The LTN is a motor nerve anatomically separated from the afferent sensory nerves (Theriault and Diamond, 1988a). The CMM reflex has been used as a functional recovery index in experimental studies of cutaneous sensory nerve regeneration in the rat (Diamond et al., 1987; Jiang et al., 2003), and in the assessment of central nervous system (CNS) regeneration following mid-thoracic spinal cord injury in which ascending parts of the reflex arc are injured (Borgens et al., 1987).

The LTN and CMM system offers a feasible and unique *in vivo* model system to study motor nerve degeneration and regeneration with experimentally induced nerve damage or with peripheral nerve diseases in mice. There has been no detailed description of the branching and innervation pattern of LTN in any species, and no studies have been done in

mice so far. Therefore we set out to (1) provide an anatomical description of the LTN and CMM in the mouse, including the pattern of LTN branching, the structure of nerve terminals and neuromuscular junctions (NMJ) in the CMM using dual labeling and transgenic mice that express a high level of yellow fluorescent protein (YFP) in their motor neurons; (2) describe the pattern of LTN degeneration following injury and of its regeneration resulting in reinnervation of the CMM; and (3) examine the pattern of degeneration in two well defined models of peripheral neuropathy. We propose that the LTN-CMM system can serve as a novel *in vivo* model for both regeneration and degeneration studies, given the simple structure and accessibility and the potential for live imaging observations.

## METHODS

### Mice

All experiments and animal care procedures were performed in accordance with the National Institutes of Health Guidelines for the Care and Use of Laboratory Animals, and were approved by the Johns Hopkins University Animal Care and Use Committee.

Two to five-month-old mice were used for the study. We utilized the YFP-transgenic mice driven by thy1 promoter elements (Thy1/YFP) (Feng et al., 2000) obtained from Jackson Labs Bar Harbor, Maine, USA (B6.Cg-Tg(Thy1-YFP)16Jrs). It is known that this transgenic line expresses YFP in the perikarya and processes of a variety of neurons, including motor neurons (Feng et al., 2000). All animals were kept in standard cages and were allowed free access to water and food. Anesthesia was induced using 4% isoflurane (Isosol, Vedco, St. Joseph, MO) and maintained throughout surgical operation using 2% isoflurane. All surgical procedures were performed under aseptic conditions. The lesion experiments consisted of three parts: 1) anatomic dissection, 2) LTN lesion to study the nerve denervation, regeneration and reinnervation to the CMM, and 3) electrophysiologic assessment of LTN function.

### Animals treated with acrylamide and the Trembler J mice

Normal adult YFP mice were treated for three weeks with acrylamide in drinking water at 400 ppm. Control mice drank regular water. Experimental procedures followed the Society of Toxicology Guiding Principles in the Use of Animals in Toxicology and National Institutes of Health (NIH) guidelines (Guide for the Care and Use of Laboratory Animals, NIH Publication No. 86-23, 1985). In addition, Trembler J mice were bred with mice expressing YFP to generate Trembler J/YFP mice to be used in assessment of neuropathy.

### Anatomical dissection

After induction of anesthesia, hair was removed from the whole body trunk from dorsal to ventral midline and from neck to tail base using an electric clipper and the commercial cosmetic depilation cream Nair®.

Whole mount preparation of back skin: Mice were deeply anesthetized and transcardially perfused with 10 ml saline followed by 50 ml of paraformaldehyde (4% in 0.1 M phosphate buffer). Whole trunk skin was dissected, postfixed in 4% paraformaldehyde for 2 h, and transferred to 0.1M PBS.

LTN: With an incision along the ventral edge of the scapula to the middle of the axilla, the LTN nerves and their origin from the brachial plexus can be observed. The LTN immediately divides into 3 main branches, namely the dorsal, lateral and ventral branches (as shown in Fig. 1a-c).

### LTN lesion in vivo

A small incision was made through the skin along the ventral edge of scapula. Care was taken not to damage the CMM. Once the CMM was exposed, an opening was made by gently separating the muscle fibers with a pair of forceps to expose all the three major LTN branches. We performed a nerve cut with a pair of iris scissors, or a nerve crush injury using a fine forceps to clamp the nerve for 30 seconds. After nerve crush injury, animals were sacrificed at 10 days (n=1), 2 weeks (n=4), 3 weeks (n=5), 4 weeks (n=5), 6 weeks (n=2) and 8 weeks (n=1) by perfusion fixation. A few more mice subjected to LTN transection were sacrificed from up to 10 days with a 24 h increment in order to study the time course of Wallerian degeneration.

### Punch skin biopsy

Under inhalation anesthesia with isoflurane, a 10×10 mm area of the back skin was depilated with Nair® cream. After cleaning with 70% alcohol, a three mm skin punch was used to obtain biopsy samples. The wound was closed by suture. The skin sample was fixed in 4% paraformaldehyde for 2 h, and transferred to 0.1 M PBS.

### Tracing the motor neuron origin of the LTN

We carried out double or triple simultaneous retrograde tracing to identify the location of the motor neurons of the 2 or 3 LTN branches using two fluorescent Alexa Fluor conjugates of Dextran (Invitrogen, Eugene, OR) and Fluoro-Gold (FG). The exposed LTN branches were cut, and the proximal cut ends were dipped in different tracers sealed in a small plastic boat sealed with Vaseline. The dorsal branch was immersed in AlexaFluor 555 (F555, 10,000 mw), the lateral branch in AlexaFluor 488 (F488, 10,000 mw), and the ventral branch in FG. Thirty minutes after tracer application, the cut ends were rinsed with saline. The wounds were closed and the animals were allowed to recover. Animals were sacrificed one week later by perfusion fixation with 4% paraformaldehyde. The cervical and rostral thoracic spinal cord were removed and processed for histology.

### Histology and Immunohistochemistry

Whole mount back skin was pre-incubated in a solution containing 0.1 M PBS, 1% Triton X-100, 5% DMSO processed and stained for motor endplates with Alexa Fluor 555-conjugated  $\alpha$ -bungarotoxin (BTX, Invitrogen, 1:1000) for 24 hrs. Additional whole mount back skins were also processed for dual staining for BTX and tyrosine hydroxylase (TH, Millipore) in order to reveal sympathetic nerve components. Whole mount skin was incubated in rabbit anti-TH (1:1000) for 24 hours, and then incubated in a mixture of Cy3 conjugated donkey anti-rabbit (Jackson Immuno, 1:500) and Alexa Fluor 647-conjugated BTX (1:1000) overnight. Punch biopsy skin samples were processed as described above for whole mount staining. Additional whole mount skins from non-YFP mice were immunostained with rabbit polyclonal antibodies against  $\beta$ -III-tubulin (1:1500, Covance) or neurofilament H (1:750, Millipore).

A portion of the initial part of the LTN and pieces of the skin representing the rostral, middle and caudal part of the back were trimmed and postfixed in 2.5% glutaraldehyde and embedded in Epon. One micron thick sections were stained with toluidine blue for light microscopy. Additional samples of the LTN branches and skin tissues were frozen in freezing isopentane and sectioned with a Cryostat. Sections were stained with antibodies against tyrosine hydroxylase (TH, Millipore) or CGRP (Millipore).

## Tissue imaging and quantification

Stained whole mount skin and sections were photographed and processed. Images were obtained using a Nikon Eclipse 80i microscope equipped with a Spot CCD camera or an AX10 Imager. M1 microscope equipped with an AxioCam HRm camera from Zeiss. Images in low magnification are composites of multiple separate images obtained successively using a 4x objective that stitched single images together using AxioVision Release 4.6 software (Zeiss). To estimate the ratio of NMJ reinnervation, we quantified 100 end plates labeled with BTX in a 1mm<sup>2</sup> square box around the DCN at a given level at T9, T12, L1, L4 and S1. End plates double labeled in yellow and connected with YFP labeled axons were counted as reinnervated NMJs. Four mice were used in each group of 2, 3 or 4 weeks.

## Functional assessment of the lateral thoracic nerve by electrophysiological analysis

Motor nerve conduction and spontaneous electromyographic activity were analysed in 3 month old YFP- transgenic control mice (n=8), and in age-matched YFP mice after proximal LTN crush (n=17). In groups of mice (controls and after 2, 4, and 6 weeks after crush) the dorsal branch of the rostro-caudal longitudinal array of the three major nerve branches (Fig. 1c) was exposed just below the scapular angle and gently freed from the surrounding skin muscle under general anaesthesia with isoflurane.

The dorsal LTN branch was stimulated with custom made bipolar electrodes (Fig. 7a). The resulting motor response in the caudal-most section of the CMM was recorded by 2×3 mm flat rectangular steel electrodes gently inserted below the skin with the firmly attached CMM through a 2 mm transverse skin incision 6 mm above the base of the tail and 6 mm sideways from the midline bilaterally. The total length of the motor nerve analysed was between 4 and 4.5 cm. First, threshold currents were determined, followed by finding the current at which the largest compound motor action potentials (CMAP) were evoked. The testing was then done with supramaximal stimuli, about 30 to 40 percent higher than the current needed to obtain maximal CMAP amplitudes. All measurements were done with at least 6 serially evoked CMAPs that were highly reproducible in size and shape. The procedures were adapted to the LTN from parts of the standard protocol developed for sciatic nerve conduction studies except that the LTN was exposed surgically here (Zielasek et al., 1996; Bremer et al., 2010). Finally, neuromuscular transmission was assessed by repetitive nerve stimulation at 3, 10, and 20 Hz adapted from an earlier sciatic nerve protocol (Toyka et al., 1975).

Following the conduction studies, spontaneous activity, an indicator of denervation, was searched for by standard electromyography (EMG) (Kimura, 2001) by using the identical pickup electrodes as for the LTN conduction studies (Fig. 7a). In contrast to standard coaxial EMG needle electrodes, our pick-up electrodes record from a much larger area of CMM fibers with high pass filter settings allowing identification of short denervation potentials such as positive sharp waves, fibrillations, fasciculation potentials, and high frequency discharges. Moreover, with these electrodes, serial measurements from the same anatomical spot can be compared to show alterations over time. Spontaneous activity (SpA) was detected by its typical shape and, in addition, by its sound pattern using the playback mode and was quantified by a simple non-linear, 4-grade ordinal scale ranging from absent to marked. Care was taken to reduce background EMG activity to near zero and thereby optimize the signal-to-noise ratio by adjusting the depth of anesthesia. Sometimes spontaneous EMG activity could not clearly be discerned from background noise and the sound recognition was the only way of identification. In another experiment five Trembler J mice were studied at age 10 weeks, and 2 at age 19 without any additional nerve lesion.

All experiments were carried out with a fully digital, laptop-based electromyography machine for human medical use (Neurosoft, Evidence 3200, Schreiber & Tholen, Stade, Germany) with program adaptations made for mouse experiments.

### Data presentation and statistical analysis

Data of NMJ reinnervation percentage are expressed as means  $\pm$  SEM. Statistical analysis employed two-way ANOVA or unpaired student's *t*-test using GraphPad Prism 5 software (GraphPad Software Inc). Values of  $P < 0.05$  were considered significant.

For the electrophysiological analysis, after re-assessment of all original recordings by an examiner unaware of the allocation to the experimental groups, the statistical calculations were done by ANOVA test with Bonferroni post-hoc corrections or with ANOVA based on ranks followed by Dunn's multiple comparison procedure depending on the distribution of Data using SigmaPlot 11 (Systat Software Inc., Chicago, USA).

## RESULTS

### I. Anatomy of the LTN and CMM

**The LTN**—We drew a schematic sketch (Fig. 1a) as a guide for the following anatomical descriptions. The LTN (Fig. 1b) is derived from the brachial plexuses. Immediately after its origin from the bronchial plexus, the LTN usually divides into three major branches (Fig 1c): here termed the dorsal, lateral and ventral branches, respectively, according to their dorso-ventral orientation. When an incision is made along the caudal edge of the scapula the LTN branches run immediately beneath the skin muscle and can be easily seen through the CMM (Fig. 1d). With this exposure, specific branches can be lesioned individually. It should be also pointed out that thick plastic sections obtained at a rostral level show that the LTN contains mostly large myelinated axons (Fig. 1b inset), similar to that described in rat (Theriault and Diamond, 1988a) and guinea pig (Blight et al., 1990).

The dorsal LTN gives rise to 2–3 branches, which run caudally in parallel and cover the dorsal and lateral parts of the trunk, whereas the lateral LTN gives rise to another 2–3 branches and cover the lateral-ventral aspect of the CMM. The ventral branch is usually smaller and sometimes splits from the pectoral nerve that is also derived from the brachial plexuses slightly proximally. The ventral LTN branch gives rise to 1–2 smaller branches innervating the ventral side of the trunk. Taken together, there are 5–8 main nerve branches running in parallel navigating caudally as shown in low magnification in Fig 1d from a YFP mouse. These branches divide further and run caudally in parallel to cover dorsal, lateral and ventral parts of the trunk (Figs. 1e–f). The midline clearly separates the left from the right side LTN (Figs. 1e–f). Thus, one side can be used as an internal control in a single whole mount preparation.

At higher magnification the majority of LTN axons and their terminals are seen brightly labeled with YFP (Figs. 1f and Fig. 2). The LTN branches extend caudally and repeatedly branch and merge such that the axonal composition of neighboring branches may change along their course. These branches give rise to many smaller ramifications, which then divide into terminal branches. The small terminal branches run transversely and form numerous irregular squares or rectangles in a meandering, mesh-like pattern (Figs. 1f and Fig 2). Terminal branches innervate endplates of the CMM as shown by labeling with the specific acetylcholine receptor marker - BTX (Fig. 2).

We also performed immunohistochemistry of whole mount skin preparations. Immunostaining for tyrosine hydroxylase (TH) in whole mount preparation labeled sympathetic axons in blood vessels and some axons running along with the cutaneous nerves

(Fig. 2a–b) but rarely in the LTN. In addition, we used whole mount back skin from normal (non-YFP transgenic) wild type mouse to examine the branching pattern of the LTN axons using immunostaining for  $\beta$ -III tubulin (Fig. 2f) or neurofilament (Fig. 2g).

LTN/CMM tissue samples can also be readily obtained using conventional 2–3 mm skin biopsy punches (Fig. 2c–e). This technique offers repeated sampling of selected areas of the LTN/CMM for spatio-temporal analyses. Whole mounts can be processed for multiple staining, revealing details of the LTN axons and terminals (Fig. 2e) and of the cutaneous sensory nerves (Fig. 2c). Each punch biopsy would provide numerous terminal branches and NMJs for examination at higher power since the whole trunk area is composed of a dense network of small and terminal LTN branches.

In this whole mount preparation, cutaneous nerves are seen running medio-laterally and perpendicular to the LTN in accordance with spinal segments (Figs. 1e–f and 2). They penetrate the CMM layer to innervate the overlying skin. From dorsal midline to ventral midline, they present dorsal, lateral and ventral cutaneous nerves, respectively (Fig. 1a and e). The branches of the LTN and cutaneous nerves can be clearly distinguished by cutting the LTN and waiting for a period sufficient for degeneration of the LTN (as shown in Fig. 5i and supplemental Fig. 3c), or labeling the tissue for TH (Fig. 2a).

**The CMM**—The CMM is a thin muscle that adheres to most of the skin of the trunk area in mice (grey shadow area in the drawing Fig. 1a) as previously described in several other species (Krogh and Towns et al., 1984; Langworthy, 1929; Theriault and Diamond, 1988a). The CMM is attached rostrally to the greater tuberosity of the humerus (Fig. 3a). This insertion differs from previous reports in guinea pig and dog in which the CMM is attached to superficial fascia around the forelimb (Blight et al., 1990; Krogh and Towns et al., 1984; Langworthy, 1929). The CMM is relatively thicker in the axillary region and spreads mediolaterally and caudally (Fig. 3a). For about 2–4 mm immediately caudal to the edge of the scapula, the muscle is still separated from the skin by a thin layer of fat. Caudal to this zone, the muscle is tightly affixed to skin. This muscle becomes a little thicker at the tail base (Fig. 3a), but less apparent than in guinea pig (Blight et al., 1990). At low magnification (Fig. 3b), numerous NMJs form clusters which appear in regular bands throughout the CMM. Transverse sections from the rostral CMM showed thicker muscle layer (Fig. 3c) than that of the middle part of the back skin (Fig. 3d). The CMM near the dorsal midline show the CMM fibers from both sides interlacing at the midline (Fig. 3d). Cryostat sections at both longitudinal (Fig. 3e) and transverse (Fig. 3f) planes showed the epidermis, dermis, LTN and TH labeled axons innervating piloerector muscles in the dermis.

**Tracing the origin of the LTN**—The LTN is derived predominantly from the ventral branches of the C7 to T1 spinal nerves, with a minor component from C6 (Fig. 4a), as confirmed by neuronal tracing. As confirmed by retrograde tracing (Fig. 4), the motor neurons contributing to the LTN are located in the ventral horn between C6–T1 segments. In the YFP strain used in this study, we observed a complete overlap of retrograde tracer labeled neurons from the LTN and YFP positive neurons (Figs. 4b and S1). We initially applied 2 different tracers to the left side LTN (F555 to the dorsal LTN branch, F488 to the lateral and ventral branches together), and a third tracer (FG) to all three branches of the right side LTN. As a result, on the left side of the cervical spinal cord we observed 2 distinct columns of labeled neurons: a medial column labeled in red from the dorsal branch and a lateral column in green from the lateral and ventral branches, whereas on the right side FG labeled neurons occupy a wider zone comparable to the combination of the 2 columns on the left side. Retrograde tracing with three different dyes (F555, FG and F488) applied to the dorsal, lateral and ventral branches of the left side LTN, respectively, revealed a clear topographical pattern corresponding to a medio-lateral position in the ventral horn as shown

on both horizontal (Fig. 4d–e) and transverse planes (Fig. 4f) between C7-T1 segments: Neurons projecting to the dorsal branches were located medially, and the neurons for the lateral/ventral branches laterally. In addition, motor neurons supplying to the ulnar and median nerves were located in the central and dorsal part of the ventral horn, distinctly dorsal to the LTN motor neurons (blue neurons in Fig. 4g). Moreover, the majority of neurons in the C6-T1 DRGs were also labeled from the ulnar and median nerves (Figs. 4g and supplemental Fig. 1). It should be noted that retrograde tracing of the LTN did not label neurons in the C6-T1 dorsal root ganglion cells (DRGs) (Fig. 4g and supplemental Fig 1), suggesting that the LTN may consist entirely of motor axons. This is similar to the findings by others in the rat (Therriault and Diamond., 1988a) and guinea pig (Blight et al., 1990).

## II. Degeneration of LTN after transection injury

Due to its large rostro-caudal extent and its branching pattern, the LTN provides a unique opportunity to study both the pathology of shorter and longer axons and of the axon terminals with their NMJs in a single whole-mount preparation.

After a proximal LTN transection (supplementary Fig. 2), Wallerian degeneration became obvious after as little as 24 hours later at terminal branches and NMJs throughout the back. The LTN trunks and larger branches, however, still appeared normal (Fig. 5a,c) and were comparable to the intact side (supplementary Fig. 2a–c). Degeneration of the presynaptic terminals and the immediate preterminal branches was more advanced in the rostral CMM (Fig. 5b) when compared to the caudal CMM (Fig. 5d). The former are innervated by the shorter LTN axons whereas the latter are innervated by longer axons. By 48 hours, NMJs of both rostral and caudal areas were denervated (Fig. 5f, h), and the larger LTN branches also showed more degeneration (Fig. 5e, g). Seven days after lesion, usually only small residues of the degenerated nerves were left (Fig. 5i). Occasionally, scattered terminal branches and even some nerve segments were observed in the distal CMM near the tail base, suggesting that degeneration of the longer motor axons might develop more slowly. We observed no LTN regeneration in the CMM 1 to 2 weeks after transection of the LTN.

In general it appears that degeneration of the major LTN trunks initiated proximally (from the transection site) and advanced distally while degeneration of terminal branches and synapses progressed earlier in the rostral part than in the caudal part of the CMM. This may indicate that the longest nerve fibers innervating the caudal CMM survive longer than the shorter axons that innervate the rostral CMM. Because labeling of endplates with BTX still persisted after nerve degeneration, it was useful for monitoring terminal degeneration and subsequently, the regeneration and reinnervation processes (Figs. 5–6).

## III. Regeneration of LTN after crush injury

In contrast to transection, we observed robust nerve regeneration 10 days after crushing the LTN. Most regenerating axons reached T10-11 dorsal cutaneous segments, i.e. about one third of the CMM, measuring about 22 mm from the beginning of proximal crush site. By 2 weeks, the regenerating axons had traversed about two thirds of the CMM, reaching the T13-L1 segmental level (Fig. 6a–c), 31 mm from the site of injury. Of note, the majority of the LTN branches regenerated at a similar pace (Fig. 6a–b). Enlargements presumably representing growth cones were visible at the tips of the regenerating nerves (Fig. 6a inset). Regenerating axons grew 43 mm and reached the L4-5 level 3 weeks following injury as shown in YFP mice and by neurofilament 200 immunostaining in non-YFP mice (Fig. 2g). By 4 weeks, regenerating LTN axons reached the base of the tail and covered virtually the entire back. We observed that NMJ reinnervation began to take place when regenerating LTN elongated distally (Fig. 6b and inset). Quantification showed that the more rostral part of the back had a higher percentage of reinnervated NMJs than the caudal regions (Fig. 6d).

We also observed sprouting of sensory and sympathetic fibers in the caudal CMM (supplementary Fig. 4f) before re-innervation by regenerating LTN axons.

We also examined sprouting by selectively dissecting an individual LTN branch (supplementary Fig. 3a–b) or transecting the whole LTN (supplementary Figs. 3c–e and 4a–e). Cutting a dorsal or lateral branch generated a distinct zone of denervation (supplementary Fig. 3a–b). Unexpectedly and in contrast to published report on the cutaneous branches (Diamond et al., 1987), even after 2 or 3 months, there was minimal sprouting from the neighboring LTN branches into the denervated zone (supplementary Fig. 3a–b). This observation, however, is in agreement with other observations in which sprouts fail to extend into denervated regions from fully innervated muscle (Gatesy and English, 1993). In addition, there was little if any sprouting across the dorsal midline after a unilateral transaction of the LTN (supplementary Fig. 3d). However, we saw robust sprouting of the sensory and sympathetic axons, at 4 week after a lesion (supplementary Figs. 3c–e and 4a–e).

#### **IV. Electrophysiological analysis shows alterations consistent with nerve-muscle pathology**

Nerve conduction was used to functionally characterize the degeneration and regeneration following crush injury. CMAP amplitudes and areas were reduced significantly by 78 % at 2 weeks after crush ( $p < 0.05$ ; ANOVA on ranks, Pairwise Multiple Comparison with Dunn's Method) and by 83 % at 4 weeks ( $p < 0.05$ ), whereas at 6 weeks and 7.5 weeks the apparent reduction was not significant when compared with the group of uncrushed control YFP transgenic mice (Fig. 7b, supplementary Fig. 5). When CMAP values of the mice with a LTN crush were compared with each other, CMAP amplitudes in mice 4 weeks after crush were significantly smaller than those in mice 7.5 weeks after crush (57%  $p < 0.045$ ; ANOVA, Bonferroni post-hoc test). Furthermore, a clear trend towards smaller CMAP was found when mice at 4 weeks post crush mice were compared to mice at 6 weeks post crush. However, this difference just missed statistical significance with the number of mice tested (51%;  $p < 0.055$ ). CMAP terminal latencies and CMAP durations were only also not significantly altered. As expected, the degree of polyphasia tended to increase (Fig. 7b). Furthermore, threshold currents and maximal currents to elicit minimal and maximal CMAP, respectively, were increased after nerve crush ( $p < 0.045$  for 2 weeks vs. 7.5 weeks; non-significant for the other comparisons), and these tended to recover over time (Supplementary Fig. 5). All these findings are in line with an axonopathic process. Neuromuscular transmission, as analysed by repetitive nerve stimulation, was not altered indicating that those motor endplates that had regained connectivity with their motor terminals became functionally normal.

After conduction and neuromuscular transmission studies were done, spontaneous EMG activity was analysed semiquantitatively as defined in Methods. From visual and acoustical assessment the mean score of increased spontaneous activity in mice 2 and 4 weeks after crush varied between mild and marked. Whereas 6 and 7.5 weeks after crush, spontaneous activity was either absent or only mild, indicating increasing reinnervation over time (supplementary Fig. 5). These observations are consistent with the anatomical pathology (see above).

#### **V. Changes in LTN in mouse models of peripheral neuropathies**

Acrylamide induced neurotoxicity is one of the better-known models of chemically induced toxic neuropathies. Acrylamide typically causes distal axonopathy of a “dying-back type” where the degeneration of axons starts distally and progresses proximally. This process is a dose-dependent phenomenon (Griffin et al., 1977; Ko et al., 2000; Nguyen et al., 2009;

Schaumburg et al., 1974). In mice treated with acrylamide, we observed that many small branches of the LTN became fragmented within 3 weeks, exhibiting a Wallerian-like degeneration (Fig. 8a). There were characteristic swellings (Fig. 8b) in the terminal branches and NMJ denervation (Fig. 8b1) in the caudal back. However, the LTN and NMJs in the rostral part of the back showed no visible signs of degeneration. As expected, the cutaneous nerves also exhibited fragmentation and ovoid-like changes, indicating that the sensory nerves also underwent Wallerian degeneration (Fig. 8a1).

In order to evaluate the utility of LTN in an inherited neuropathy model, we examined the nerve pathology of the Trembler J mouse, a classic model of Charcot-Marie Tooth disease type 1, a common human hereditary disorder. Its phenotype is characterized by myelin loss and axon degeneration caused by a molecular defect of Pmp22 (Ayers et al., 1975; Zielasek and Toyka 1999). We observed few abnormalities in the rostral back of 3 months old Trembler J mouse. However, the caudal back revealed degeneration of small branches and marked denervation of the NMJs (Fig. 8c–d). Axonal swelling (Fig. 8d1) and pre-terminal degeneration (Fig. 8d2) were seen in the middle of the back. Using electrophysiology, in five 10-week old Trembler J mice, motor latencies were markedly increased by a factor of up to 10 (Trembler J:  $4.6 \text{ ms} \pm 2.6$ ; wild type control  $0.47 \text{ ms} \pm 0.2$ ;  $p < 0.002$ ), the CMAP amplitudes and areas were reduced by over 50 percent (Trembler J:  $200 \mu\text{V} \pm 0.22$ ; wild type control  $556 \mu\text{V} \pm 0.38$ ;  $p < 0.013$ ; Fig. 7b), and the CMAP duration was doubled (Trembler J:  $11.6 \text{ ms} \pm 4.8$ ; wild type control:  $5.3 \text{ ms} \pm 0.85$ ;  $p < 0.003$ ; Fig. 7b), as expected for a disorder affecting myelin sheaths and axons. These abnormalities were much more pronounced in 19-week old trembler mice ( $n=2$ , Fig. 7b).

## DISCUSSION

In the present study, we examined the anatomical and functional characteristics of the LTN/CMM system and showed that it could serve as a novel neuromuscular system to study motor nerve degeneration and regeneration in mice. Its feasibility and usefulness was demonstrated in three experimental paradigms: nerve injury, toxic neuropathy and a common genetic neuropathy. In addition to its potential value in a wide range of experimental studies, by means of serial punch biopsies the LTN/CMM system has the added inherent potential for longitudinal studies, a useful feature for testing new treatment strategies for peripheral neuropathies and nerve regeneration.

In line with previous studies in rat (Theriault and Diamond, 1988a) and guinea pig (Blight et al., 1990), we did not observe any neurons in the C6-T1 DRGs that were labeled by tracer injected into the LTN or CMM. This suggests that the nerve fibers in the LTN are likely to be exclusively motor. In contrast, the sensory and autonomic innervation of the back is provided by segmental, dorsal and lateral cutaneous nerves (Blight et al., 1990; Theriault and Diamond, 1988a, 1988b). The CMM is only a few fibers thick, allowing the labeling and staining of all structures of interest in whole mount preparations without further dissection. Neuromuscular junctions are scattered along the entire length of the CMM. This characteristic feature facilitates the quantification of the spatiotemporal sequence of NMJ denervation and reinnervation at the same time with motor nerve degeneration or regeneration, both morphologically and functionally. Furthermore, the LTN/CMM system is amenable to classical electrophysiological techniques. We observed a good correlation between our electrophysiological and anatomical observations. A further strength of the method is that serial electrophysiological studies can be performed in individual animals with very good precision and reproducibility. Conduction velocities can be approximated by motor latencies but measurements of nerve conduction velocities with more than one nerve stimulation site are less well defined or even precluded because of the many crossings of

small branches in and out of the epineurium of the rostrocaudal main branches (Toyka and Grünewald, unpublished observations, 2011).

The motor nucleus of the LTN is somatotopically organized in the mouse as previously described in rat (Therault and Diamond, 1988b) and dog (Krogh and Towns, 1984). These previous studies and our present data show that the rostrocaudal arrangement of the motor neurons is reflected in the rostrocaudal level of the muscle fibers that they innervate. The mediolateral position of the LTN motor neurons is also somatically organized. In transverse sections of the spinal cord, the positions of the motor neurons that accumulate retrogradely transported tracers reflect the distance from the midline of the injected muscle fibers. Importantly, we observed that the entire population of retrogradely labeled neurons is YFP positive, suggesting that all of the LTN axons are labeled by YFP in the Thy1-YFP strain. This would directly validate the quantitative comparison analysis for nerve degeneration, regeneration and reinnervation between treatments.

One clear advantage of the LTN system is to provide anatomical and functional compartments in one preparation to simultaneously study the progression of degeneration and regeneration in nerve trunks and terminals of both longer and shorter axons. The branching pattern of the LTN and the distinct and non-overlapping muscle regions innervated by the LTN conform to classical descriptions of neuromuscular compartments (English and Letbetter, 1982; English and Weeks, 1984). Our observation that degeneration initiated in the most distal nerve terminals and proceeded in a caudorostral direction is in agreement with majority of previous reports on how Wallerian degeneration and NMJ denervation takes place after nerve injury (Lubicka, 1977; Lunn et al., 1990; Miledi and Slater, 1970). Although throughout the whole CMM, terminal branches and the smaller ramifications degenerated earlier than main branches or nerve trunks, we observed a slower pace of degeneration of the NMJs and small branches in the caudal CMM that are derived from the longer axons, in comparison to the degeneration in the rostral CMM that is innervated by the shorter axons. This is in line with earlier observations using the phrenic nerve lesion model that the time of NMJ degeneration depended on the length of the distal stump (Miledi and Slater, 1970). Moreover, we observed that the main branches or nerve trunks in the rostral CMM degenerated faster than those in the caudal CMM, indicating that the degeneration process for the nerve trunks initiates proximally and progresses distally, similar to earlier observations in the CNS (George and Griffin, 1994) and in the PNS (Beirowski et al., 2005) after nerve transection. This is different from the degeneration process in the compartment of terminals and small collaterals. Therefore, the current model system might help to resolve the contradictions and anomalies with regard to directionality of Wallerian degeneration reported in the early literature.

One of the advantages of the LTN model for regeneration studies is that it allows one to observe rate of axonal regeneration in a relatively homogenous motor neuron population. Following a crush injury, the LTN regenerated robustly and the majority LTN axons regenerated at a relatively homogenous pace. This might be reflected by the fact the LTN constitutes axons of similar size axons and originates from a relatively similar size of motor neuron pool. Our data showed that the speed of axonal elongation was slower at later time measurements (>3–4 weeks) than that observed during the early period (10 days to 2 weeks). Demonstration of this decline in the regeneration rate at later time points and in longer axons will likely have important implications for human nerve regeneration as axons are often tasked with regenerating over much longer distances. As a preclinical tool, model of nerve regeneration in the LTN could easily be used to test for drugs that can enhance nerve regeneration in longer axons.

Using previously established models of peripheral neuropathies induced by either neurotoxic chemicals or pathogenic mutations, we showed that the LTN is particularly useful to examine patterns of nerve degeneration. Mice treated with acrylamide for 3 weeks demonstrated LTN axonal neuropathy with more severe axonal degeneration in the caudal back area, resembling the dying-back pathology as previously shown in mixed sensory-motor nerves (Ko et al., 2000; Suzuki and Pfaff 1973). Similarly, the LTN/CMM system revealed axonal degeneration and NMJ denervation in the Trembler J mouse. Both axonal and pre-synaptic swelling were observed in acrylamide treated and in Trembler J mice. These degenerative features were more pronounced in the caudal back, supporting a previous description of distal degeneration (Ayers et al., 1975). Relative ease of the preparation and examination of both short and long axons in models of peripheral neuropathies lends itself to preclinical proof-of-concept trials of potential neuroprotective drugs.

In studies looking into the spatiotemporal sequence of fiber degeneration and regeneration, the sciatic nerve with its sensory, motor and autonomic fibers, has been widely used in the mouse and rat. However, this model system has some disadvantages. The sciatic nerve innervates many different muscles and muscle fiber types through its complex branching pattern making it more difficult to evaluate the pathobiology of lesions or diseases. For functional assessment of motor regeneration, recovery of toe spreading (Garcia et al., 2009), ankle dorsiflexion (Garcia et al., 2009), or combined measures assessing footprint and foot pressure (Vogelaar et al., 2004) while walking, or using video gait analysis (Yu et al 2001) can all be utilized. However, the branching pattern can result in faulty regeneration that limits functional recovery, or the gait disorder as a principal read-out system may be contaminated by lesion-induced neuropathic pain (Vogelaar et al., 2004), autotomy (Kingery et al., 1989), or by contractures (Baptista et al., 2007).

As a purely motor nerve, injury to the LTN is unlikely to produce neuropathic pain. The most attractive advantage of the LTN and the anatomy of the CMM is that this preparation is amenable to novel treatments with a wide range of compounds including novel molecular inhibitors, anti-inflammatory mediators, neurotrophic factors and the like, both *in vivo* by placement of osmotic minipumps with catheters and *ex vivo* in organ bath preparations.

Some of the advantages of the LTN/CMM model are inherent in the anatomy of the system. Other advantages are less intuitive. Temperature is a factor that has received little attention, but represents a potential confound in assessing the speed of regeneration. We found that the nerve bed of the denervated mouse hind foot is much cooler than that of unoperated animals, but that the temperature of the CMM did not alter following LTN lesion as measured on the overlying skin surface for 3 weeks (Pan and Griffin, unpublished observations, 2010). The processes of both axonal transport (Cancalon, 1985; Gross et al., 1975) and of Wallerian degeneration (Tsao et al., 1999) are known to be temperature-dependent, so that temperature-related changes in either could affect the outcome of treatment studies.

Recent advances in understanding the biology of axonal degeneration (Groh et al., 2010; Knöferle et al., 2010; Nave and Trapp, 2008) have promoted research into developing small molecules or biological agents that could protect axons in disease (Nikolaev et al., 2009) or speed up regeneration. The discovery of transcription factors and other control molecules that influence regeneration in injured neurons (Seiffers et al., 2007), the renewed interest in growth factors, and of inhibitory molecules derived from myelin debris, and the extracellular matrix collectively call for a simple and reliable experimental model to be biologically tested. We propose that the LTN/CMM system may be promising in this respect, in particular when studying transgenic mouse models.

In summary, the LTN/CMM model allows for easy dissection and manipulation, shows minimal morbidity, and is amenable to quantitative assessment of degeneration, regeneration and reinnervation by recovery of the CMM reflex and by segmental CMAP's. Moreover, repeated combined skin and CMM biopsies can be feasibly done to serially examine the time to degeneration and regeneration for any rostrocaudal region of interest in a given animal. This model holds promise for future preclinical studies of potential neuroregenerative or neuroprotective drugs.

## Supplementary Material

Refer to Web version on PubMed Central for supplementary material.

## Acknowledgments

We thank Kimberly Brown for plastic embedding and Dr. Paul Hoffman for helpful discussions and input. This study was supported by NIH (NS41269), Packard Center for ALS Research, Dr. Miriam and Sheldon G. Adelson Medical Research Foundation and Muscular Dystrophy Association grants and by intramural research funds of the University of Würzburg.

## REFERENCE LIST

- Ayers MM, Anderson R. Development of onion bulb neuropathy in the Trembler mouse. Comparison with normal nerve maturation. *Acta Neuropathol.* 1975; 32:43–59. [PubMed: 1146506]
- Baptista AF, Gomes JR, Oliveira JT, Santos SM, Vannier-Santos MA, Martinez AM. A new approach to assess function after sciatic nerve lesion in the mouse - adaptation of the sciatic static index. *J Neurosci Methods.* 2007; 161:259–264. [PubMed: 17204334]
- Beirowski B, Adalbert R, Wagner D, Grumme DS, Addicks K, Ribchester RR, Coleman MP. The progressive nature of Wallerian degeneration in wild-type and slow Wallerian degeneration (Wlds) nerves. *BMC Neurosci.* 2005; 6:6. [PubMed: 15686598]
- Blight AR, McGinnis ME, Borgens RB. Cutaneous trunci muscle reflex of the guinea pig. *J Comp Neurol.* 1990; 296:614–633. [PubMed: 2358554]
- Borgens RB, Blight AR, McGinnis ME. Behavioral recovery induced by applied electric fields after spinal cord hemisection in guinea pig. *Science.* 1987; 238:366–369. [PubMed: 3659920]
- Bremer J, Baumann F, Tiberi C, Wessig C, Fischer H, Schwarz P, Steele AD, Toyka KV, Nave KA, Weis J, Aguzzi A. Axonal prion protein is required for peripheral myelin maintenance. *Nat Neurosci.* 2010; 13:310–318. [PubMed: 20098419]
- Canalón P. Influence of temperature on various mechanisms associated with neuronal growth and nerve regeneration. *Prog Neurobiol.* 1985; 25:27–92. [PubMed: 2417280]
- Carter LM, Starkey ML, Akrimi SF, Davies M, McMahon SB, Bradbury EJ. The yellow fluorescent protein (YFP-H) mouse reveals neuroprotection as a novel mechanism underlying chondroitinase ABC-mediated repair after spinal cord injury. *J Neurosci.* 2008; 28:14107–14120. [PubMed: 19109493]
- Diamond J, Coughlin M, Macintyre L, Holmes M, Visheau B. Evidence that endogenous beta nerve growth factor is responsible for the collateral sprouting, but not the regeneration, of nociceptive axons in adult rats. *Proc Natl Acad Sci USA.* 1987; 84:6596–6600. [PubMed: 3306683]
- English AW, Letbetter WD. A histochemical analysis of identified compartments of cat lateral gastrocnemius muscle. *Anat Rec.* 1982; 204:123–130. [PubMed: 7181128]
- English AW, Weeks OI. Compartmentalization of single muscle units in cat lateral gastrocnemius. *Exp Brain Res.* 1984; 56:361–368. [PubMed: 6479269]
- Feng G, Mellor RH, Bernstein M, Keller-Peck C, Nguyen QT, Wallace M, Nerbonne JM, Lichtman JW, Sanes JR. Imaging neuronal subsets in transgenic mice expressing multiple spectral variants of GFP. *Neuron.* 2000; 28:41–51. [PubMed: 11086982]
- Fu SY, Gordon T. The cellular and molecular basis of peripheral nerve regeneration. *Mol Neurobiol.* 1997; 14:67–116. [PubMed: 9170101]

- Garcia ML, Rao MV, Fujimoto J, Garcia VB, Shah SB, Crum J, Gotow T, Uchiyama Y, Ellisman M, Calcutt NA, Cleveland DW. Phosphorylation of highly conserved neurofilament medium KSP repeats is not required for myelin-dependent radial axonal growth. *J Neurosci.* 2009; 29:1277–1284. [PubMed: 19193875]
- Gatesy SM, English AW. Evidence for compartmental identity in the development of the rat lateral gastrocnemius muscle. *Dev Dyn.* 1993; 196:174–182. [PubMed: 8400403]
- George R, Griffin JW. The proximo-distal spread of axonal degeneration in the dorsal columns of the rat. *J Neurocytol.* 1994; 23:657–667. [PubMed: 7861182]
- Giovannelli Barilari M, Kuypers HG. Propriospinal fibers interconnecting the spinal enlargements in the cat. *Brain Res.* 1969; 14:321–330. [PubMed: 5794910]
- Griffin JW, George EB, Chaudhry V. Wallerian degeneration in peripheral nerve disease. *Baillieres Clin Neurol.* 1996; 5:65–75. [PubMed: 8732200]
- Griffin JW, Price DL, Drachman DB. Impaired axonal regeneration in acrylamide intoxication. *J Neurobiol.* 1977; 8:355–370. [PubMed: 70511]
- Groh J, Heintz K, Kohl B, Wessig C, Greeske J, Fischer S, Martini R. Attenuation of MCP-1/CCL2 expression ameliorates neuropathy in a mouse model for Charcot-Marie-Tooth 1X. *Hum Mol Genet.* 2010; 19:3530–3543. [PubMed: 20591826]
- Gross GW, Biedler LM. A quantitative analysis of isotope concentration profiles and rapid transport velocities in the C-fibers of the garfish olfactory nerve. *J Neurobiol.* 1975; 6:213–232. [PubMed: 52689]
- Hall S. Nerve repair: a neurobiologist's view. *J Hand Surg Br.* 2001; 26:129–136. [PubMed: 11281664]
- Heine W, Conant K, Griffin JW, Höke A. Transplanted neural stem cells promote axonal regeneration through chronically denervated peripheral nerves. *Exp Neurol.* 2004; 189:231–240. [PubMed: 15380475]
- Höke A. Mechanisms of Disease: what factors limit the success of peripheral nerve regeneration in humans? *Nat Clin Pract Neurol.* 2006; 2:448–454. [PubMed: 16932603]
- Holstege G, Blok BF. Descending pathways to the cutaneous trunci muscle motoneuronal cell group in the cat. *J Neurophysiol.* 1989; 62:1260–1269. [PubMed: 2600623]
- Jiang S, Khan MI, Wang J, Middlemiss PJ, Werstki ES, Wickson R, Rathbone MP. Enteric glia promote functional recovery of CTM reflex after dorsal root transection. *Neuroreport.* 2003; 14:1301–1304. [PubMed: 12876461]
- Kimura, J. Types of electromyographic abnormalities. In: Kimura, J., editor. *Electrodiagnosis in Diseases of Nerve and Muscle: Principles and Practice.* Oxford; 2001. p. 339-369.
- Kingery WS, Vallin JA. The development of chronic mechanical hyperalgesia, autotomy and collateral sprouting following sciatic nerve section in rat. *Pain.* 1989; 38:321–332. [PubMed: 2812843]
- Knöferle J, Koch JC, Ostendorf T, Michel U, Planchamp V, Vutova P, Tönges L, Stadelmann C, Brück W, Bähr M, Lingor P. Mechanisms of acute axonal degeneration in the optic nerve in vivo. *Proc Natl Acad Sci USA.* 2010; 107:6064–6069. [PubMed: 20231460]
- Ko MH, Chen WP, Hsieh ST. Cutaneous nerve degeneration induced by acrylamide in mice. *Neurosci Lett.* 2000; 293:195–198. [PubMed: 11036194]
- Krogh JE, Towns LC. Location of the cutaneous trunci motor nucleus in the dog. *Brain Res.* 1984; 295:217–225. [PubMed: 6713184]
- Langworthy OR. A morphological study of the panniculus carnosus and its genetical relationship to the pectoral musculature in rodents. *Am J Anatomy.* 1925; 35:283–302.
- Lubińska L. Early course of Wallerian degeneration in myelinated fibres of the rat phrenic nerve. *Brain Res.* 1977; 130:47–63. [PubMed: 884520]
- Lunn ER, Brown MC, Perry VH. The pattern of axonal degeneration in the peripheral nervous system varies with different types of lesion. *Neuroscience.* 1990; 35:157–165. [PubMed: 2359492]
- Miledi R, Slater CR. On the degeneration of rat neuromuscular junctions after nerve section. *J Physiol.* 1970; 207:507–528. [PubMed: 5499034]
- Nave KA, Trapp BD. Axon-glial signaling and the glial support of axon function. *Annu Rev Neurosci.* 2008; 31:535–561. [PubMed: 18558866]

- Nguyen T, Mehta NR, Conant K, Kim KJ, Jones M, Calabresi PA, Melli G, Hoke A, Schnaar RL, Ming GL, Song H, Keswani SC, Griffin JW. Axonal protective effects of the myelin-associated glycoprotein. *J Neurosci*. 2009; 29:630–637. [PubMed: 19158290]
- Nikolaev A, McLaughlin T, O’Leary DD, Tessier-Lavigne M. APP binds DR6 to trigger axon pruning and neuron death via distinct caspases. *Nature*. 2009; 457:981–989. [PubMed: 19225519]
- Raivich G, Makwana M. The making of successful axonal regeneration: genes, molecules and signal transduction pathways. *Brain Res Rev*. 2007; 53:287–311. [PubMed: 17079020]
- Schaumburg HH, Wi niewski HM, Spencer PS. Ultrastructural studies of the dying-back process. I. Peripheral nerve terminal and axon degeneration in systemic acrylamide intoxication. *J Neuropathol Exp Neurol*. 1974; 33:260–284. [PubMed: 4362700]
- Seiffers R, Mills CD, Woolf CJ. ATF3 increases the intrinsic growth state of DRG neurons to enhance peripheral nerve regeneration. *J Neurosci*. 2007; 27:7911–7920. [PubMed: 17652582]
- Suzuki K, Pfaff LD. Acrylamide neuropathy in rats. An electron microscopic study of degeneration and regeneration. *Acta Neuropathol*. 1973; 24:197–213. [PubMed: 4357171]
- Theriault E, Diamond J. Intrinsic organization of the rat cutaneous trunci motor nucleus. *J Neurophysiol*. 1988a; 60:463–477. [PubMed: 3171638]
- Theriault E, Diamond J. Nociceptive cutaneous stimuli evoke localized contractions in a skeletal muscle. *J Neurophysiol*. 1988b; 60:446–462. [PubMed: 3171637]
- Toyka KV, Drachman DB, Pestronk A, Kao I. Myasthenia gravis: passive transfer from man to mouse. *Science*. 1975; 190:397–399. [PubMed: 1179220]
- Tsao JW, George EB, Griffin JW. Temperature modulation reveals three distinct stages of Wallerian degeneration. *J Neurosci*. 1999; 19:4718–4726. [PubMed: 10366605]
- Vogelaar CF, Vrinten DH, Hoekman MF, Brakkee JH, Burbach JP, Hamers FP. Sciatic nerve regeneration in mice and rats: recovery of sensory innervation is followed by a slowly retreating neuropathic pain-like syndrome. *Brain Res*. 2004; 1027:67–72. [PubMed: 15494158]
- Yu PR, Matloub HS, Sanger JR, Narini P. Gait analysis in rats with peripheral nerve injury. *Muscle Nerve*. 2001; 24:231–239. [PubMed: 11180206]
- Zielasek J, Martini R, Toyka KV. Functional abnormalities in P0-deficient mice resemble human hereditary neuropathies linked to P0 gene mutations. *Muscle Nerve*. 1996; 19:946–952. [PubMed: 8756159]
- Zielasek J, Toyka KV. Nerve conduction abnormalities and neuromyotonia in genetically engineered mouse models of human hereditary neuropathies. *Ann N Y Acad Sci*. 1999; 883:310–320. [PubMed: 10586256]

### Highlights

Evaluation of nerve degeneration and regeneration is difficult in rodents

We developed a new model of nerve degeneration and regeneration

This new model uses lateral thoracic nerve (LTN) and cutaneous maxims muscle (CMM)

Degeneration and regeneration of LTN can be monitored both temporally and spatially

The LTN/CMM is suitable for both regeneration and studies

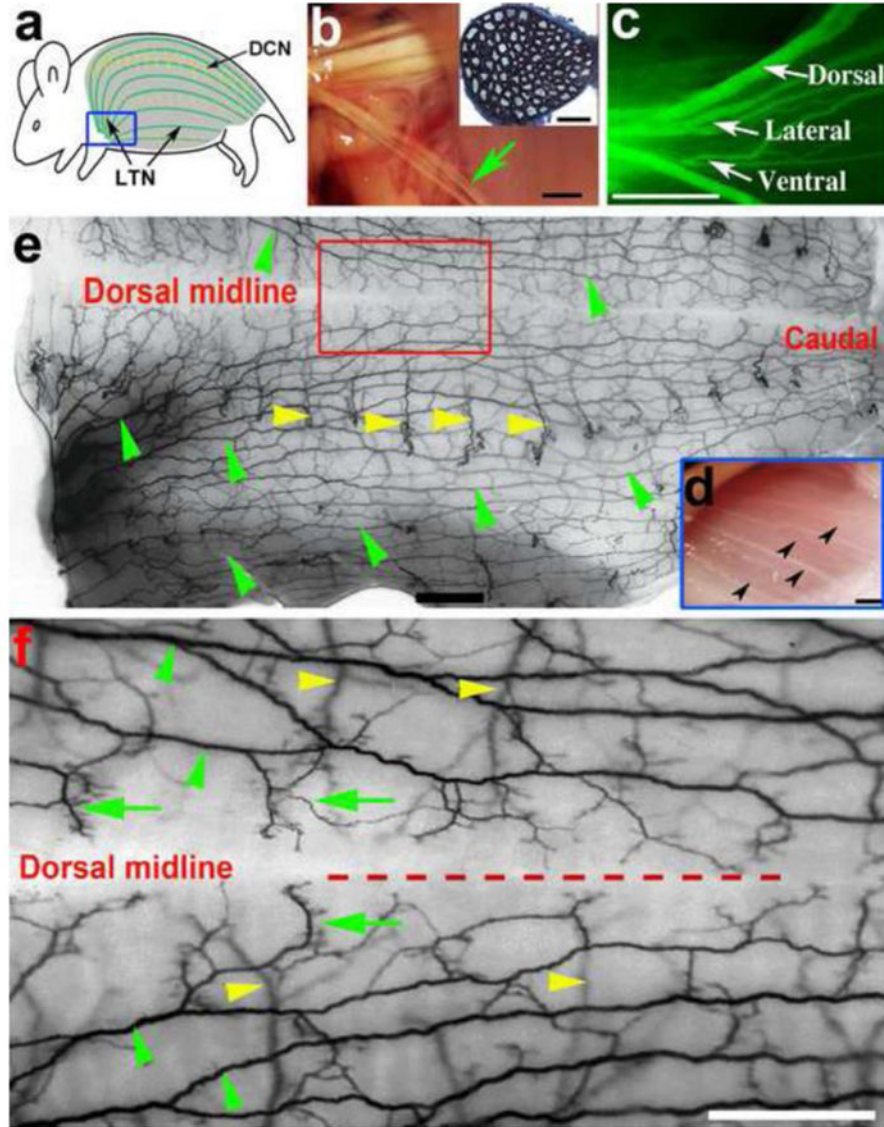


**Figure 1.**

Anatomy of the LTN. a: Schematic drawing of the mouse back showing the CMM (shadow area), LTN (green lines) and DCN (yellow broken lines). b shows the LTN is derived from the brachial plexuses. Green arrow points to the LTN. Inset is one micron plastic section through a LTN branch stained with toluidine blue shows rather uniform myelinated axon caliber. c: Major LTN branches (dorsal, lateral and ventral) from an YFP mouse examined through a fluorescent dissection microscope. d: Surgical microscope view of the LTN branches through translucent CMM after an incision along the scapula. The area corresponds to the blue rectangle in (a). e: Inverted black and white image of half of the trunk (right side) from an YFP mouse showing LTN running horizontally (green arrowheads) and branching net. Yellow arrowheads mark example DCN. Caudal is to the right. f: Higher power view of the dorsal middle back to reveal small and terminal branches, and the midline, top half is left side. Green arrows indicate LTN terminal branches, other symbols are the same as in e. Note a clear midline zone separating the left and right side. LTN, lateral thoracic nerve; CMM, cutaneous maximus muscle; DCN, dorsal cutaneous sensory nerve. Scale bars: 2 mm for b, c, d, e, f; 100  $\mu\text{m}$  for b inset.

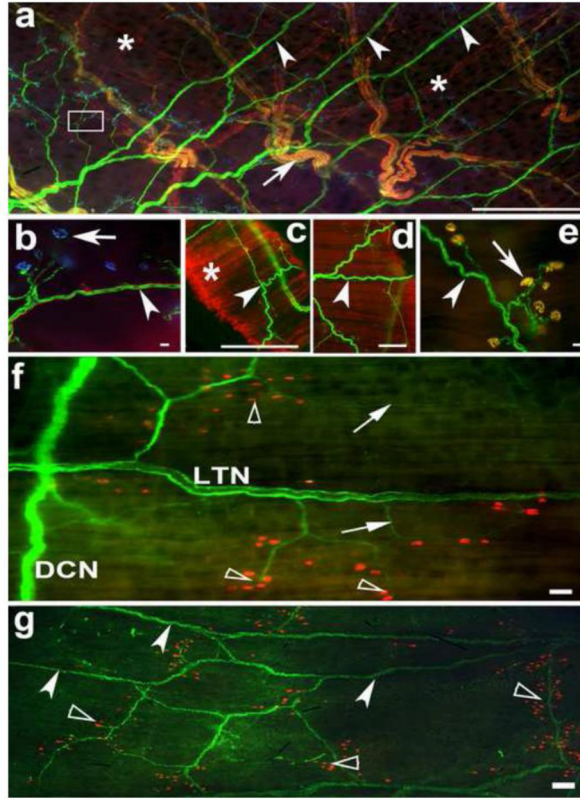


**Figure 2.**

Whole mount immunostaining of the LTN-CMM system a: Whole mount back from a YFP mouse was immunostained for TH (red) and BTX (blue). LTN are in green (white arrow heads), DCN nerves were strongly labeled for TH (merged with YFP in yellow, arrow) and TH-labeled sympathetic axons were marked with asterisks. The small white box was amplified in (b) to show NMJs (arrow). Arrowhead indicates a LTN branch. c–e: Punch skin biopsy from the mid-back stained in whole mount for BTX. c: low power view. Arrowhead points to the LTN branches, asterisk indicates the CMM. d: terminal branches and NMJs are visible at higher power (arrow). e: high power view shows small branches (arrowhead) and NMJs (arrow). f: LTN-CMM preparation from a non-YFP mouse, LTN axons are labeled in green by immunostaining with rabbit anti- $\beta$ -III tubulin, and NMJs in red labeled by BTX. Arrows indicate small LTN branches; arrowheads point to NMJs. g: Whole mount tissue of the caudal back from a non-YFP mouse stained with neurofilament H (green) and BTX (red). LTN, lateral thoracic nerve; CMM, cutaneous maximus muscle; DCN, dorsal cutaneous sensory nerve. Scale bar: a, c = 2 mm, d = 500  $\mu$ m, b and e = 100  $\mu$ m, f = 200  $\mu$ m, g = 400  $\mu$ m.

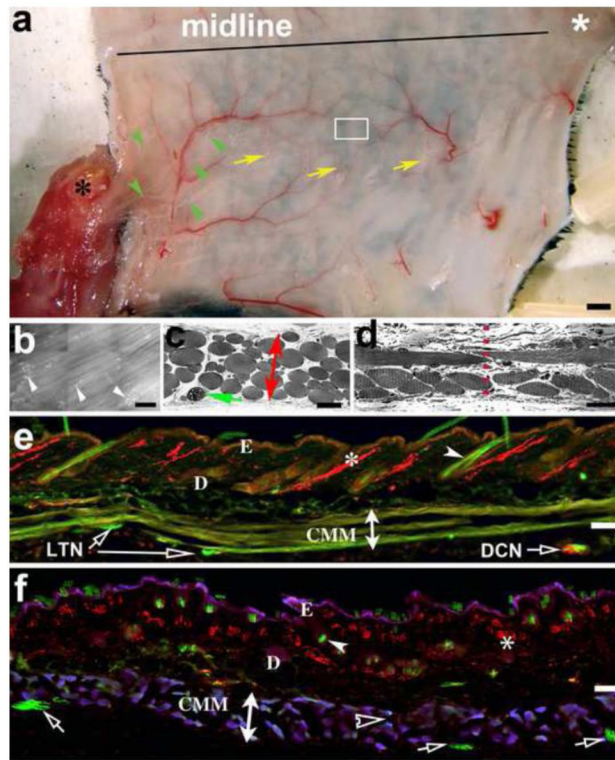


**Figure 3.**

The CMM system a: Whole skin and CMM preparation with right-side forelimb attached. Note that the CMM originates from the humerus bone (black asterisk) and spreads to cover the trunk. Horizontal line indicates the midline. LTN branches (green arrow heads) and DCN (yellow arrows) are visible. White asterisk marks the tail base. b: black and white image of the CMM taken from the box in (a) shows whole mount stained with BTX to label NMJs (white arrowheads), muscle fibers can be seen in background. c shows toluidine-blue stained plastic embedded muscle fibers of the CMM layer in a transverse section from the rostral back. Green arrow indicates a LTN branch in transverse plane. Red bidirectional arrow shows the thickness of the CMM layer. d: A transverse section through the dorsal midline of the CMM showing interlace of muscle fibers at midline structure (dashed red line). e–f: Vertical cryostat sections cut longitudinally (e) or transversely (f) showing the epidermis (E), dermis (D), and the thin layer of the CMM. The CMM layer and small LTN branches (empty arrows) can be seen. Asterisk indicates TH labeled sympathetic axons, filled arrowheads point to hair shafts in both e and f; empty arrowhead in (e) points to NMJs. LTN, lateral thoracic nerve; CMM, cutaneous maximus muscle; DCN, dorsal cutaneous sensory nerve. Scale bars: a=2 mm, b–f = 100  $\mu$ m.

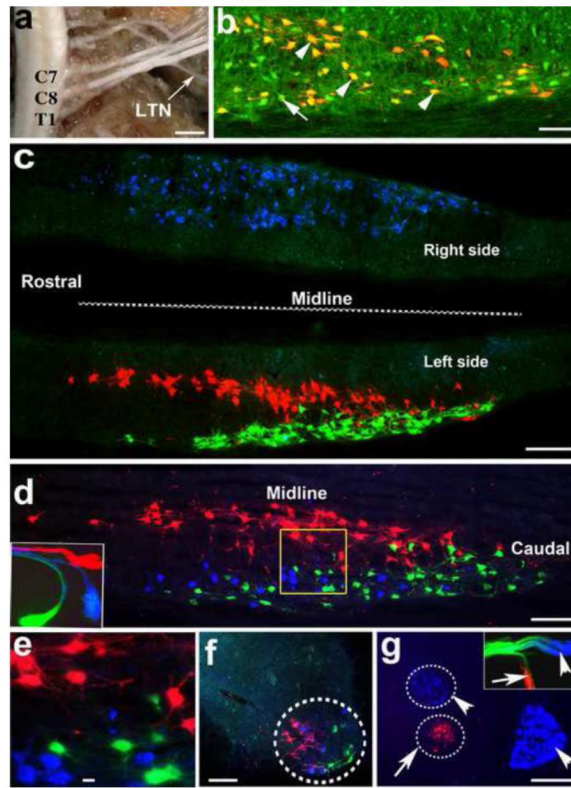


**Figure 4.**

Tracing the origin of LTN a: Dissection of the cervical cord and the branchial plexus. LTN is seen as a small branch derived from the branchial plexus. b: Horizontal section of the C7-8 spinal cord ventral horn shows tracer (red) labeled neurons from the LTN are overlapped with YFP-tagged neurons (green). Arrowheads point to double-labeled neurons, and arrow points to YFP single-labeled neuron. c: Horizontal section through the ventral horn of C6-T1 segments showing both left side and right side of the cord following bilateral LTN tracing. Left side has 2 separate columns of neurons labeled in red (medial) and green (lateral) representing tracing from the dorsal and lateral-ventral branches separately, whereas the right side shows symmetrically a group of neurons labeled by FG from the right side LTN. d: the topographic pattern of labeled neurons in red, blue and green representing tracing from the dorsal, lateral and ventral branches, respectively, with triple tracing technique from a unilateral LTN. Inset shows the three branches of the left side LTN labeled by different tracers. The yellow box was amplified in higher magnification (e) to show the labeled neurons. There are no double or triple labeled neurons. f: Labeled neurons from the three LTN branches are located mediolaterally in a C8 transverse section. g: Distinct location of the LTN neurons labeled in red with a tracer applied to the whole LTN (stained in red and pointed by a white arrow in the inset) from neurons innervating the forelimb (median and ulnar nerves labeled in blue with another tracer - FG pointed by arrowhead in the inset). Scale bars: a=2 mm; b-g = 100  $\mu$ m.

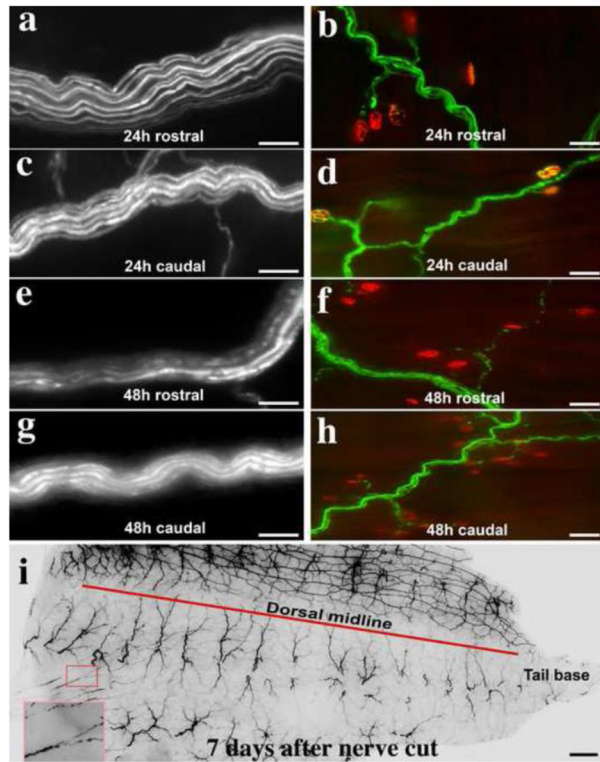


**Figure 5.**

LTN degeneration after transection a–b: appearance of a nerve trunk (a) and terminal area (b) in the rostral CMM at 24h after injury. c–d: Less advanced degeneration in the distal CMM in both nerve trunk (c) and terminals (d). e–h: more advanced degeneration at 48h after nerve cut. The distal CMM showed slower terminal degeneration (g–h) than the rostral part (e–f). i. Few remnants of LTN left at 7 days after injury (inset). The segmental sensory nerves (DCN) are clearly visible below the red line. Scale bars = 50 μm for a, c, e, and g; = 100 μm for b, d, f, h; = 2 mm for i.

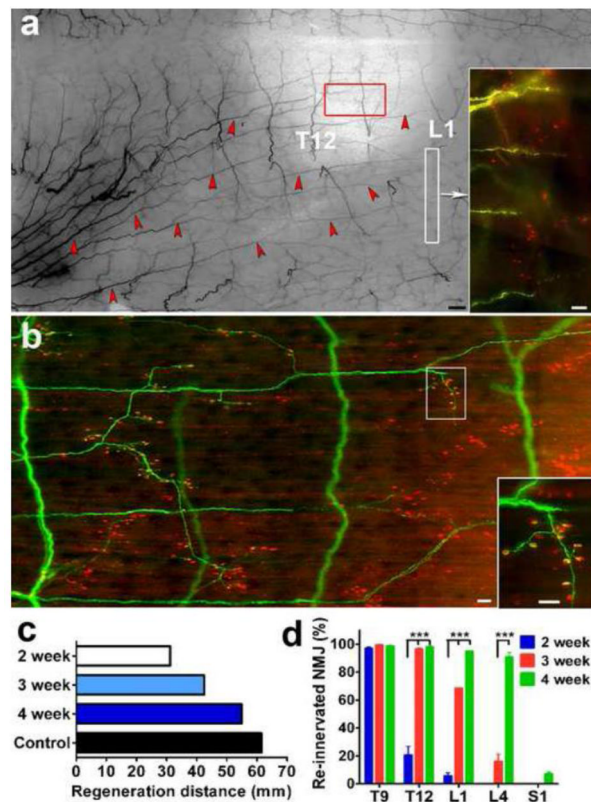


**Figure 6.**

Regeneration of LTN after crush injury a: LTN axons regenerate and grow caudally (to the right). The majority of nerve fibers grew in a similar pace and reached the L1 spinal level at 2 weeks. White vertical rectangle shows tips of growing axons in inset. b: is from the red rectangle in (a), showing more details of the growing axons and the re-innervation process. Branching and NMJ re-innervation are further shown in details (inset). c: Spatiotemporal progression of LTN regeneration. d: Quantification (percentage) of re-innervated NMJs from several representative regions: T9-10; T12-13; L1-2; L4-5, and S1-2. Scale bars = 1 mm for a; = 100  $\mu$ m for a inset, b and b inset. \*\*\* denotes  $p < 0.001$ .

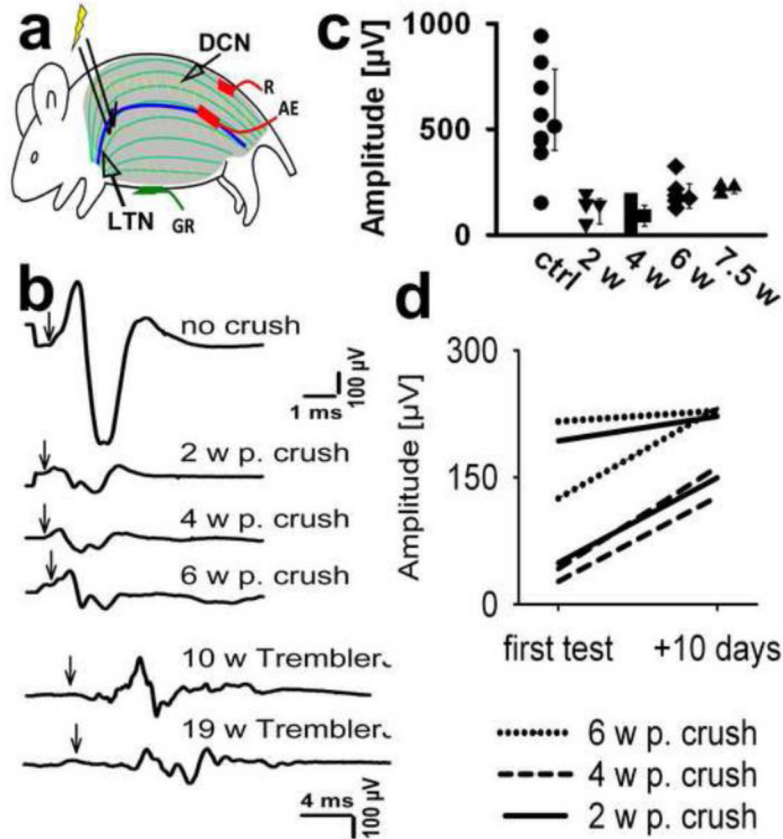


**Figure 7.**

Electrophysiology a: Schematic drawing of the electrophysiology setup with LTN stimulation and dorsal skin muscle pick up electrodes. b: Representative CMAP recordings upon LTN stimulation from a non-crushed control mouse and from 3 individual mice at different time intervals after nerve crush. Amplitudes decrease markedly and increase gradually with longer time intervals. The lowermost two traces show representative recordings from a 10 week-old and a 19 week-old Trembler J mouse showing a profound and over time progressive slowing of nerve conduction, note the change in sweep speed. Arrows indicate onset of CMAPs, defining motor latency. c: CMAP amplitudes upon LTN stimulation in groups of mice after nerve crush. At 2 weeks after nerve crush, and occasionally thereafter, CMAP amplitudes are lowest and improve gradually over 6 weeks. Median values of 4–6 consecutive measurements for every animal, grouped according to post crush time, as well as medians of groups. Error bars: 75th and 25th percentile, respectively). d: CMAP amplitudes of serial recordings after nerve crush: Two mice each were measured at 2, 4 or 6 weeks after crush and all six were re-evaluated a second time 10 days later. Functional improvement of the CMAP amplitudes over the 10-day period is depicted. The two obtained data points are median values of 4–6 consecutive measurements in each animal at indicated time points. LTN: lateral thoracic nerve; CMAP: compound muscle action potential; R: reference pick up electrode; AE: active pick up electrode; GR: ground electrode; W denotes weeks post crush.

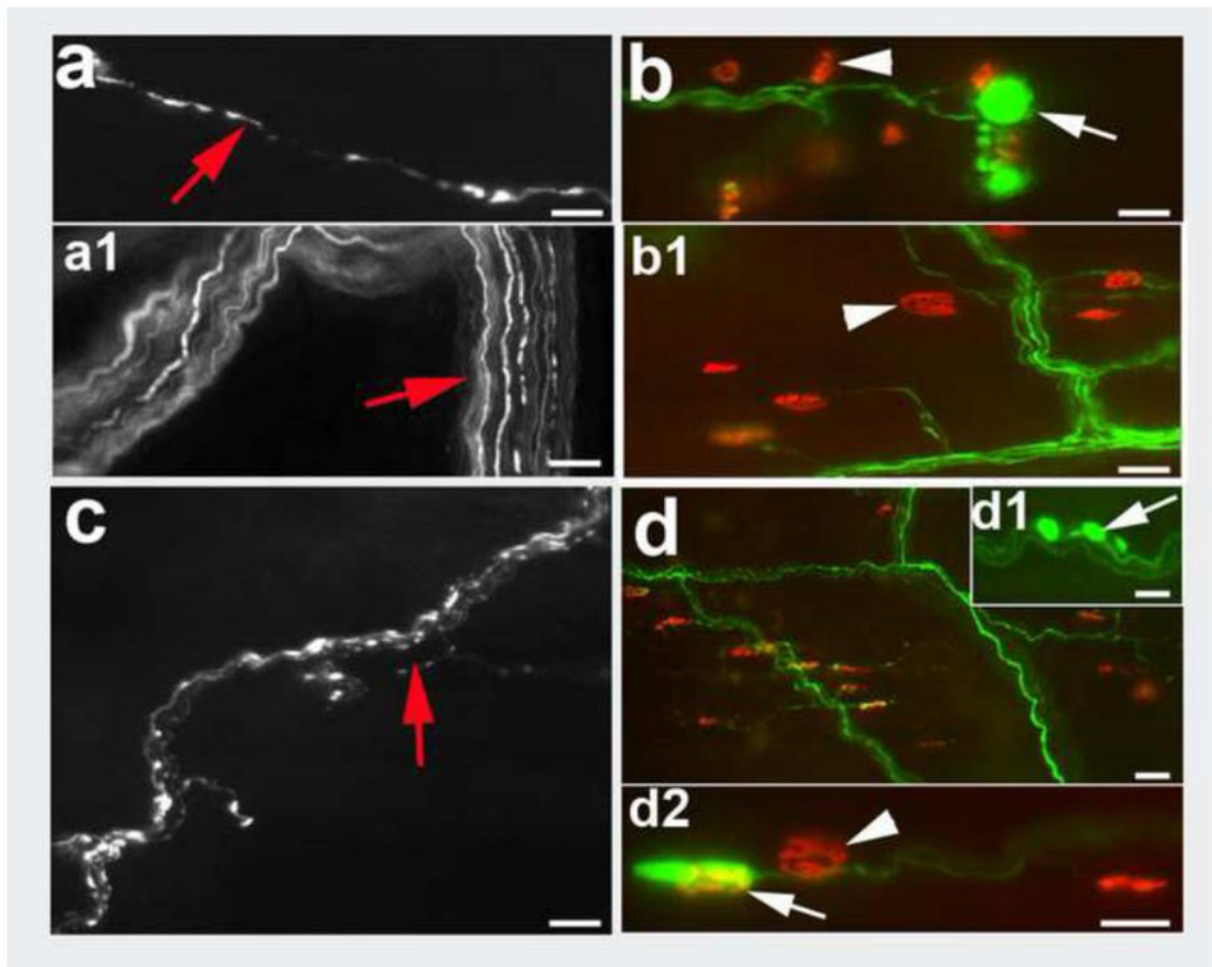


**Figure 8.**

LTN degeneration in peripheral neuropathy models a–b: Acrylamide induced neuropathy in the caudal back. a: fragmented LTN branches, a1 degenerated cutaneous sensory nerve; b: terminal swelling and NMJ denervation (b1); c–d: Sample images of LTN degeneration in a Trembler J mouse. c shows many small LTN branches undergoing severe degeneration. d: degenerated axons and denervated NMJs, insets show swelling of axons (d1) and of a pre-terminal axon segment at higher magnification (d2). Scale bars = 20  $\mu\text{m}$  for left side panels (a, a1 and c); = 50  $\mu\text{m}$  for all the right side panels (b, b1, d, d1, and d2).